Recent Results of Riga Group on Laser Applications for Skin Diagnostics

J. Spigulis*, V. Lukinsone, I. Oshina, E. Kviesis-Kipge, M. Tamosiunas, A. Lihachev

Biophotonics Laboratory, Institute of Atomic Physics and Spectroscopy, University of Latvia, Jelgavas 3, Riga, LV-1004, Latvia

* janis.spigulis@lu.lv

Abstract. Laser-related activities of Biophotonics Laboratory at UL Institute of Atomic Physics and Spectroscopy, following the previous *ICSQE-2018* conference, are reviewed. Four recent research projects are considered, including one EC Horizon-2020 project, two European Regional Development Fund (ERDF) projects and one project funded by the Latvian Council of Science (LCS). The projects are generally aimed at development of new optical methods and technologies for non-invasive *in-vivo* skin assessment to facilitate early diagnostics of skin malformations (including cancers). Most of the projects explore novel approaches of camera-based biomedical imaging for clinical diagnostics and recovery monitoring.

1. Introduction

A brief review about the activities of Biophotonics laboratory on lasers for skin assessment following the previous *ICSQE-2018* conference will be presented. The main projects under implementation are:

1) *Multimodal imaging technology for in-vivo diagnostics of skin malformations*, ERDF #1.1.1.1/18/A/132;
2) *Development of prototype devices for nonivasive assessment of skin condition*, ERDF #1.1.1.2/VIAA/1/16/070;
3) *Time-resolved autofluorescence methodology for non-invasive diagnostics of skin cancer*, ERDF #1.1.1.2/VIAA/1/16/014;
4) *Advanced spectral imaging technology for skin diagnostics*, LCS # lzp-2018/2-0006.

The first project aims at development of a combined method for skin diagnostics involving picosecond laser applications for time-dependent optical characterization of skin (autofluorescence lifetimes, fluorescence lifetime imaging, time-of-flight spectroscopy, skin-remitted photon path lengths). Values of the remitted photon path lengths at particular wavelengths and input-output distances are important for several clinical applications including reflection pulse oximetry and skin chromophore mapping. They can be estimated by modelling; however, there are very few experimental data available to validate the simulations. Models mostly consider distribution of path lengths for all photons independently of their travel directions and interactions within the tissue. One can expect that the total path length of the survived skin-remitted photons should be longer than the mean path length related to all photons launched in the tissue (were a certain amount of them is absorbed). Systematic experimental studies on spectral and spatial dependencies of the skin-remitted

photons are needed to quantitatively answer this question. Our measurements were taken using specific optical fiber contact probes from *in-vivo* skin, both healthy and pathologic, and from agar-based skin phantoms. Besides, Raman spectra and Raman spectral band images from ex-*vivo* skin samples under the 785 nm laser excitation were studied in frame of the first project.

In the second and fourth projects, different concepts of multi-spectral-line imaging are implemented in new prototype devices for skin chromophore mapping and autofluorescence imaging. One design comprises an illumination ring of laser diodes around the image capturing camera. Another one employs a silica-core side emitting fibre loop as simultaneous four spectral line illumination source, combined with double-camera setup or with a single VIS-NIR four-band camera. Besides, skin autofluorescence is excited by violet 405 nm laser diodes and detected in the G-band of RGB camera. Unfortunately, clinical validation phase of the prototypes is somewhat delayed due to restrictions related to the Covid-19 pandemic. The third project investigates origins of the photo-bleaching of laser-excited skin autofluorescence.

2. Methods and Equipment

In the first project, a measurement set-up shown in Fig.1 was used. The time-correlated single photon counting method was applied for optical pulse shape measurements. A broadband picosecond laser (*Whitelaser micro supercontinuum lasers, Fianium, NKT PHOTONICS, DK,* 400-2000 nm, pulse full width at half maximum 6 ps, repetition rate 20 MHz) was used as initial light source. Time resolution of the system was 9.7 ps which ensured minimum detectable photon path length ~2 mm. Specific narrow spectral bands were selected by couples of identical interference filters. One of them was filtering the input light while the other was placed in front of the photo-detector (photomultiplier HPM-100-07 combined with the detector controller DCC-100 and data processing card SPC-150, all *Becker&Hickl GmbH,* DE). The estimated the temporal resolution of the system was ~ 5 ps which causes ~ 1 mm error of the determined photon path lengths. The examined spectral range was 560-800 nm; the spectral bands were selected with a 40 nm step using 10 nm half-bandwidth interference filters (*Andover Corporation, USA* - part numbers 560FS10-12,5; 600FS10-12,5; 640FS10-12,5; 680FS10-12,5; 720FS10-12,5; 760FS10-12,5; 800FS10-12,5).

Stable recording of optical signals via the input and output fibers (WF-400, *Light Guide Optics International*, LV, silica core diameter 400 microns, length 1,05 m) was ensured by means of a custom-made fiber holding probe with inter-fiber distances 1 mm, 8 mm, 12 mm, 16 mm and 20 mm. To provide equal pressure on the skin surface at all measurements, the probe was designed as a lift where the inside sliding part with the couple of fibers lied on the skin, providing a pressure determined by its weight ~ 35 g/cm^2. The outside part of the probe was fixed on skin during the measurements. In

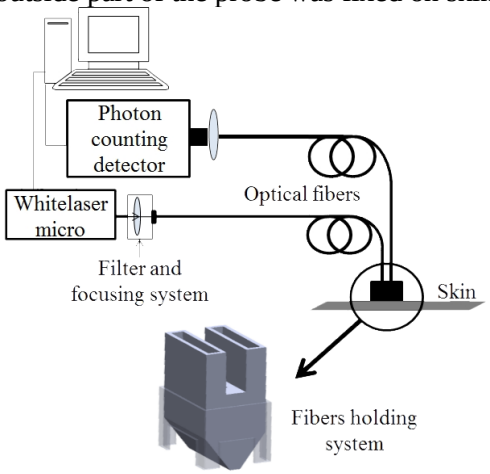

Figure 1. The picosecond pulse reflectance measurement set-up.

order to verify how much variation does probe pressure cause in the mean photon path lengths, additional series of measurements at two wavelengths (760 nm and 800 nm) and all five inter-fiber separations were taken applying three probe-skin pressures – 35 g/cm^2, 112 g/cm^2 and 224 g/cm^2. The observed variations did not exceed 5 %.

Ten volunteers with skin photo-type II or III (Fitzpatrick classification), aged between 25 and 68, were examined with their written consent under permission of the local Ethics Committee. The measurements were taken from healthy skin of the forearm, avoiding contact with large superficial blood vessels. The average spectral power on skin was ~10 mW/cm^2, i.e. well below the skin laser safety limit 200 mW/cm^2 [1].

Processing of the measured data involved comparing the shapes of skin input and output pulses - *a(t)* and *b(t)*, respectively. The temporal distribution function *f(t*) of photon arrivals following infinitely narrow δ-pulse input were found by de-convolution of the integral

$$b(t) = \int_0^t a(t-\tau) f(\tau) d\tau \qquad (1).$$

This inverse problem was solved using a built-in deconvolution algorithm of *Matlab*. As the de-convolved function was more noisy than *b(t)*, original scripts were developed for data smoothing using the *Log-normal* function, as well as for semi-automatic calculations of the temporal distribution functions and the mean arrival times of skin-scattered photons. In particular, the output signal *b(t)* was fitted by *Log-normal* distribution function using non-linear fitting Matlab *lsqcurvefit* algorithm. This function was selected due to its similarity to the measured data. Next, the input pulse was shifted in time towards output pulse until the rising fronts of pulses coincided at the 5% level. The path length of the first detected photons was obtained as: *Min path length = dt c/n* , where *dt* is the time shift towards output pulse. Then the inverse problem (1) was solved using a built-in Matlab deconvolution algorithm *deconv* and *f(t)* was calculated. Finally, the mean arrival time of skin-scattered photons was calculated as the time moment when the area under curve *f(t)* equals from left and right side. After restoring *f(t)*, the corresponding distribution of back-scattered photon path lengths in skin was calculated as

$$\phi(s) = f(t) \cdot c/n \qquad (2),$$

where *c* is the speed of light in vacuum and *n* is the mean refraction index of superficial skin tissues (n ~ 1.4 [2]). The photon mean path lengths in skin were found as the mean values of integrated path length distribution functions. Eventual error due to different slopes of both rising fronts (after the time-shifting) did not exceed 2 mm.

Recently we proposed and tested a new multispectral imaging modality where illumination of the target (e.g. skin) is performed by multiple laser-emitted spectral lines instead of spectral bands. We have demonstrated that up to three spectral line images can be extracted from a single snapshot RGB image data set under simultaneous triple-wavelength illumination [3-5]. Recently a four spectral line imaging double-camera prototype (Fig.2) was designed, assembled and tested [6]. Illumination system comprised two laser modules (1) – RGB module emitting ~ 20 mW at each of the three spectral lines (450 nm, 523 nm, 638 nm) and a NIR 850 nm / 40 mW module. As a patented novelty, several semi-elliptical loops of side emitting optical fiber attached to the laser modules were exploited as light source ensuring uniform multi-laser illumination of the target area via a polarizing film. Two cameras (RGB and NIR, MQ022CG-CM and MQ022RG-CM respectively, *Ximea, DE*) equipped with 425 nm and 800 nm long-pass filters (mod. #84-742 and #66-235, *Edmund Optics*, GB, respectively) and orthogonally oriented input polarizers are capturing simultaneously images of the same skin area. Four spectral line images are subsequently extracted from the image data for further calculation of four chromophore distribution maps using the previously developed methodology [7]. Within a second the laser modules are switched off and skin autofluorescence (AF) image at the G-channel of RGB camera is captured under illumination by four 405 nm, 40 mW laser diodes (DL-5146-101S, *Roithner*, AT), in order to discriminate skin melanoma from seborrheic keratosis [8]. The recorded images can be seen on the display (5.5inch HDMI AMOLED, *Waveshare*, CN) or transmitted via SBC's *wi-fi* to the remote computer for calculation of chromophore maps or performing other tasks. The device is fully self-sustained by using rechargeable Li-ion batteries (INR18650-25R, *Samsung*, KR) as the power

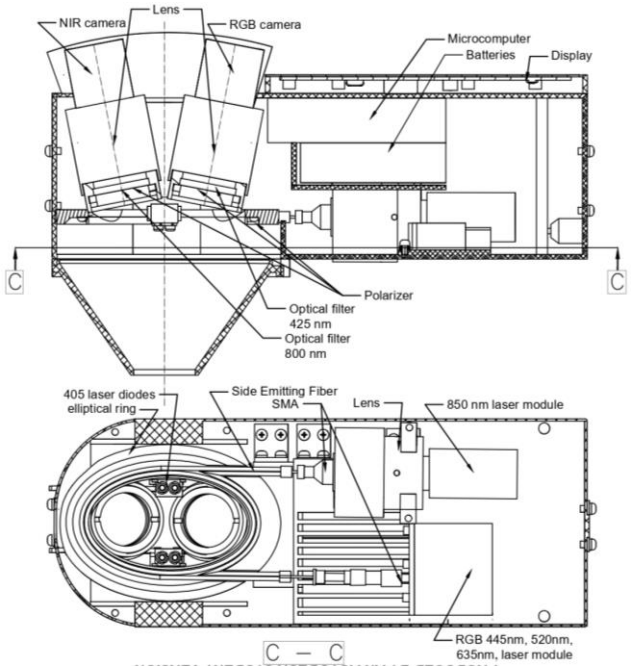

Figure 2. Design scheme of the 4+1 laser wavelengths prototype device [6].

supply.

Another recent design [9] allowed consecutive capturing of five spectral line images within 4 seconds using a laser diode ring illuminator (Fig.3,a). Device functioning (Fig.3,b) is based on *Windows CE 7.0* operating system; it has built-in processing software for nearly real-time calculation of skin chromophore maps. In total, 20 laser diodes emitting at five wavelengths (405, 450, 520, 660, and 850 nm) and 4 white LEDs for preview mode are operated. Each set of equal lasers is powered separately by a constant current laser driver. A system on chip module *Nvidia Tegra 2 T20* with a 1 GHz dual core *ARM Cortex-A9* processor is used as a central processing unit. 3 Mpix RGB CMOS matrix serves as the image sensor, connected to a central processor via a 10-bit parallel line. The image sensor has 10-bit ADC which provides1024 grades of intensities for each spectral image. Mini USB connector and SD memory card are used for image transfer to external computer. All low level tasks are laid down to 32-bit Arm-based *Cortex®-M4 STM32L4* series microcontroller. It is programmed as I2C interface slave device and emulates RTC chip. Pushbutton tasks are embedded in

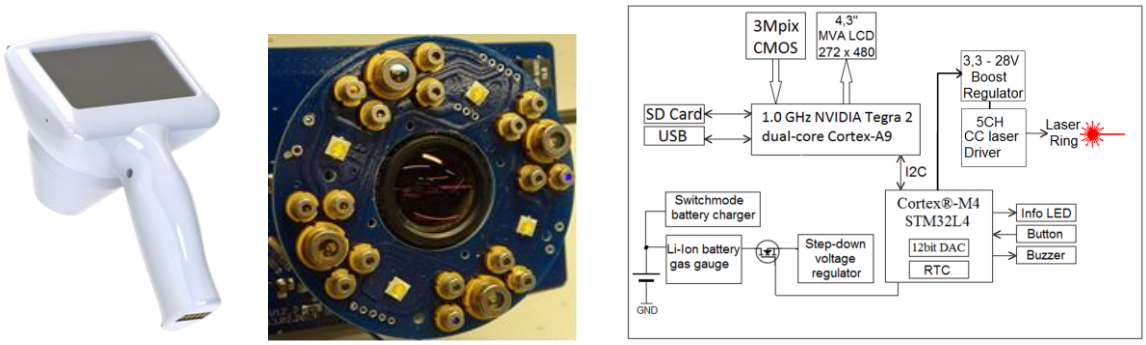

a b c

Figure 3. Outlook (a), design details (b) and functional scheme (c) of the recent five spectral line imaging prototype [9].

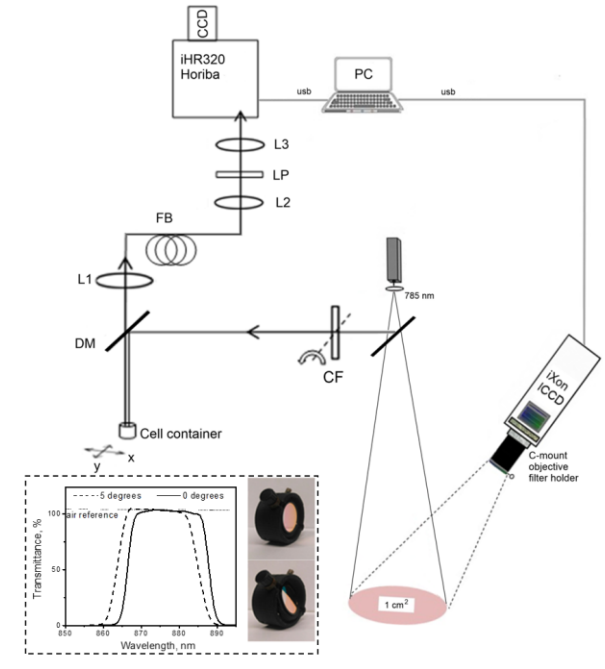

Figure 4. Combined set-up for acquisition of Raman macro images and spectra. Intensified CCD camera (iXon Ultra 888, Andor) records Raman images through the set of optical filters embedded into the filter holder, including 785 nm laser rejection filter and rotated band pass filter positioned at 0 degrees or at 5 degrees perpendicular to the optical axis. Additional components: CF – laser clean-up filter; DM – dichroic mirror; L1 – fiber coupling lens; L2, L3 – collimating lenses; FB – fiber bundle; LP – long pass filter ($OD_{785\ nm}$ >6); xy – translational stage. The transmittance spectra of tunable band pass filter were measured by using DU 800 (Beckman Coulter, Brea, CA, USA) spectrophotometer. software.

Dimensions of the device are 121 x 205 x 101 mm, weight ~ 440 g.

A case study for non-melanoma skin cancer diagnosis was included in the Raman scattering research project. Raman spectroscopy and imaging data were obtained from human squamous cell carcinoma (SCC), basal cell carcinoma (BCC), nevus and surrounding skin samples, *ex vivo*. Raman spectra were recorded by iHR320 imaging spectrometer equipped with 1200 g/mm grating and thermoelectrically cooled Syncerity-CCD camera (Horiba, Japan). A 785 nm diode laser excitation was delivered to the sample by fiber optics, used together with the filter sets to adjust output fluency to 40 mW/cm^2 and to filter out fiber silica bands, including the dichroic filter serving to reflect/reject excitation light and to transmit the Raman signal (Fig.4). The imaging system comprised iXon Ultra 888 EMCCD camera (DU-888U-CS0-#BV, Andor Technology, UK), 785 nm excitation notch filter (NF03-785E-25, Semrock, USA) and the narrow-band optical filter (FF01-880/11-25, Semrock, USA) attached to macro lens (35mm focal length, f/2.8 - f/16, Edmund Optics). Angular adjustment of narrow-band filter produced ~3 nm Anti-Stokes shift at 90% of transmittance level. The final image of Raman scattered light was computed by subtracting two images transmitted at peak different wavenumbers, thereby removing the background autofluorescence of the sample.

Cell preparation for Raman spectroscopy and autofluorescence measurements: dc-3f or b16f10 cells were cultured as monolayer in DMEM (supplemented with 10% fetal calf serum, 1% l-glutamine, 100 μg/ml streptomycin and 100 u./ml penicillin), incubated at 37 °C with 5% CO_2 and air. Shortly

before the measurements, the cells were trypsinized, re-suspended in 1x PBS, centrifuged and the pellet of approx. 6×10^6 cells was transferred into a bottom flat cylinder container (h = 3mm; r = 2,5 mm V = 50 µl) tightly covered inside with 24" gold folia. The fiber bundle comprising a single excitation fiber and 6 collection fibers (NA = 0.22) was positioned at 25 mm distance from the cell sample surface. For conducting the Raman spectral measurements on the dead cells, the cells were stored in PBS at 4 ^{o}C, up to 1 month. For conducting autofluorescence measurements, the cells were incubated with singlet oxygen sensor green (SOSG) reagent (Promega Corp., USA) at 5 µM final concentration and affected with light for 10 minutes at 30 mW/cm^2 power density. SOSG fluorescence was estimated in cell supernatant under the 473 nm excitation.

3. Results

In result of kinetic skin remittance measurements, nearly linear dependences of the remitted photon mean path length on inter-fibre distance were obtained for all wavelength bands, while the spectral dependences at fixed inter-fibre distances showed more complicated character, most probably due to absorption of the dermal haemoglobin (Fig.5). More results of this study are published in [10].

Fig.6,a illustrates the obtained data on photon mean path length through healthy skin and skin neoplasms. The data was calculated as the mean values from 6 measurements (skin and pigmented nevi of diameter 8-11 mm). As expected, increased inter-fibre distance, as well as increased wavelength, has led to increased photon path length. However, we did not observe essential differences in their values if healthy skin and neoplasms are compared. We noticed that photon path length increases on body locations with more fat, which also results in increased error of average data for all measurements at longer wavelengths and larger distances between fibres.

Fig. 6,b illustrates the mean photon path length dependencies in phantoms. The phantoms comprised two different concentrations of additives, first was with 1% of intralipid concentration and second with 1% of haemoglobin. The results were obtained for 4 wavelengths (520, 560, 680 and 760 nm) at 5 different distance between fibres (1, 8, 12, 16 and 20 mm). Haemoglobin is the main absorber in human skin below 600 nm. As expected, in phantoms with haemoglobin the mean photon path length is shorter if compared with that in phantoms without haemoglobin.

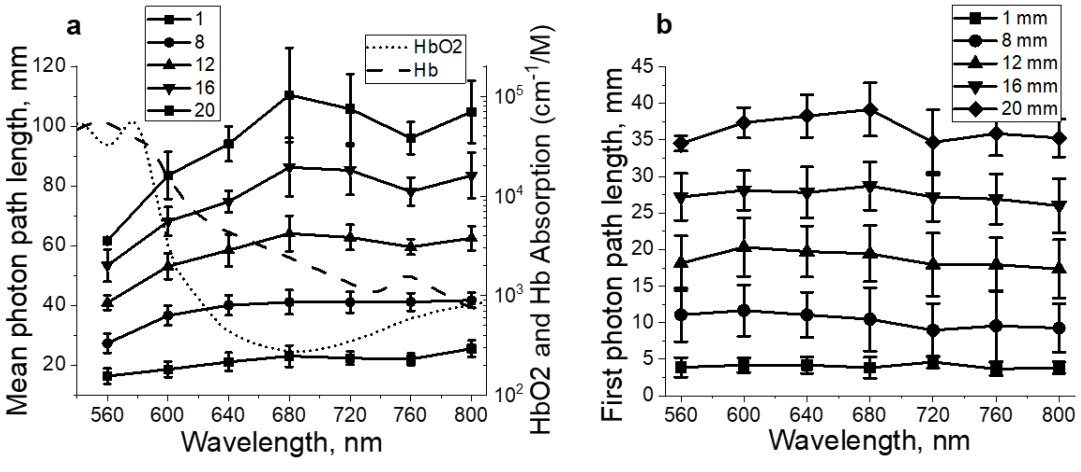

a b

Figure 5. a - spectral dependencies of the mean path length of skin-remitted photons at various inter-fiber distances, b – spectral dependencies of the path lengths calculated for the first-arrived photons (detected at 5% level of output pulse maximum). The dotted curves in (a) represent absorption of oxy- and deoxy-haemoglobin [10].

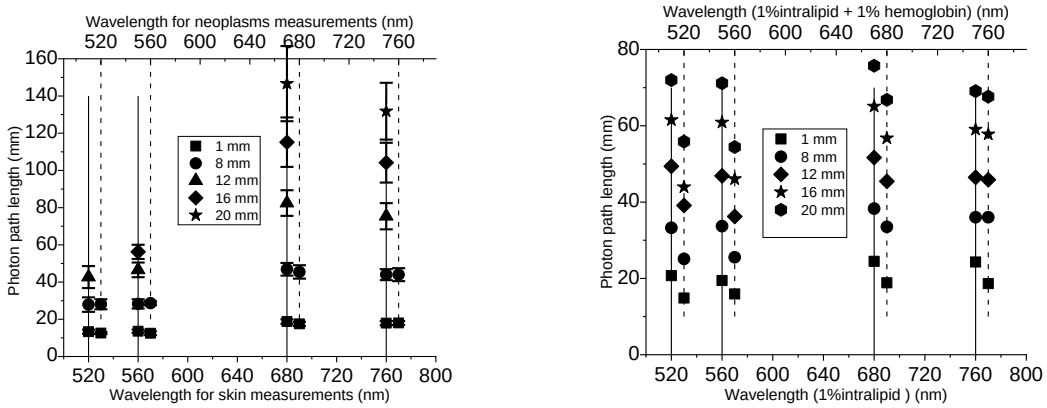

a b

Figure 6. a - the mean remitted photon path lengths in skin (–) and neoplasms (--); b - the data for phantoms with 1% of intralipid concentration (–) and with 1% of intralipid and 1% of haemoglobin concentration (--) [11].

Leading towards Raman's scattering results, the obtained spectra of skin were composed of Raman vibrational modes of proteins, lipids, and amino acids. Skin cancer induced changes of these components, reducing Raman band intensities near 1300 cm^{-1} and 1450 cm^{-1} (Fig. 7). In line with the previous studies [12, 13], Raman signal reduction in BCC and SCC skin cancer indicated lower amount of collagen and elastin (1271 cm^{-1}, 1452 cm^{-1}), also lower content of ceramide and triolein lipids (1301 cm^{-1}, 1440 cm^{-1}). Decrease of intensity at 1450 cm^{-1} corresponds to a change in molecular composition of proteins.

Raman macro imaging results confirmed the decreased Raman intensity of BCC and SCC cancer in comparison to the healthy skin (Fig. 8). Considering the filter transmittance at >90 % level, the filter rotation at 0 degrees (or at 5 degrees) allow capturing Raman image at 1217 – 1456 cm^{-1} (or at 1185 – 1409 cm^{-1}) wavenumber interval. Thus, the differential image extracts the Raman band intensity alterations at 1409 – 1456 cm^{-1} wavenumber interval, particularly corresponding to the decrease of Raman band intensity near 1450 cm^{-1} related to the developed skin cancer. For explanation, tumor-

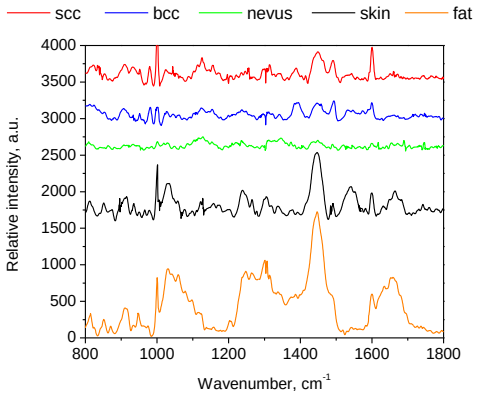

Figure 7. Measured mean Raman spectra of skin, subcutaneous fat tissue, nevus and skin cancer (SCC and BCC). The intensity axis offset is induced for clarity.

secreted metalloproteinases induced the degradation of collagen and prohibited pro-collagen biosynthesis. Less triolein could be due to lowering of subcutaneous volume of fat during the lesion formation [13].

Our data also showed that Raman spectral features of nevus can be more likely related to BCC or SCC than to normal skin (Fig. 7). Thus, the imaging results are not cancer-specific, as Raman images of nevus display reduced intensity compared to the skin. However, we emphasize that Raman signal reduction is a temporal process, significantly affected by the occurrence of cell death. It has been shown previously that decrease of the Raman band intensity near 1450 cm^{-1} occurs due to the cell death (necrosis) [14]. We observed that decrease in 1450 cm^{-1} peak intensity (dominated by proteins and lipids) is consistent with malignant transformation, independently of the tissue type (BCC or SCC). Further results obtained *in vitro* were used to model the Raman spectral changes related to the time course of cell death. The decrease of the whole Raman spectrum intensity at 1448 cm^{-1} was observed in dead cells (Figure 9). As shown in Figure 9 (insert) the data points approximated with mono-exponential decay provided time (9 days) to decrease the 1448 cm^{-1} band intensity to 37% of its initial value. As already described [14], the degradation of the lipid membranes occurs first, resulting the significant decrease in Raman intensity from lipid compounds measured in the dead cells at 24 -72 hours. The peak residuals can be ascribed to the protein content, however no comparison to previous work is available for relating Raman spectra intensity decrease to the changes in protein and lipid structure alterations at longer times.

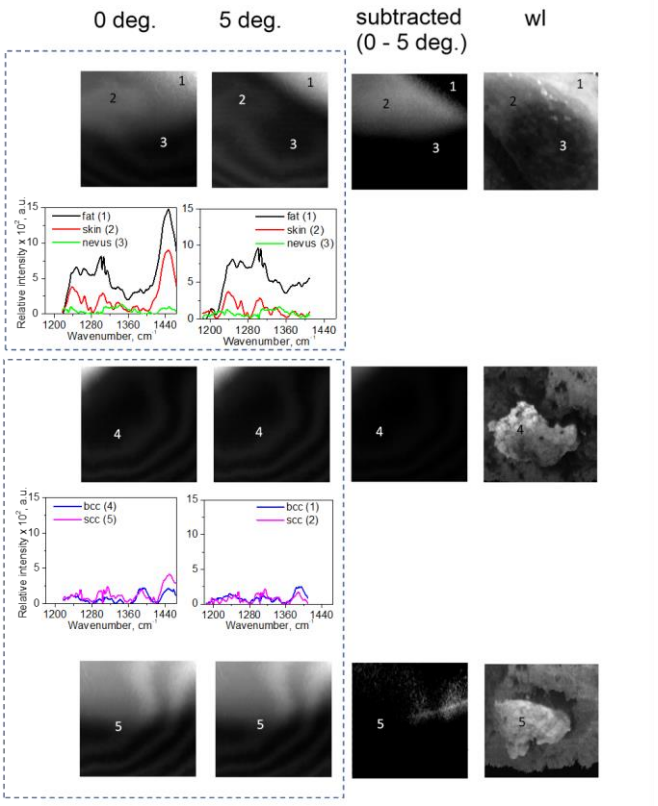

Figure 8. Top view of Raman macro images at 0 degree and 5 degree filter turning and white light images, *ex vivo*. Numbers on imaging data denote tissue morphological localization: 1 – subcutaneous fat; 2 – skin; 3 – nevus; 4 – BCC; 5 - SCC. The subtracted images (5 deg. from 0 deg.) are depicted in the middle column. To interpret the relative image intensity values, the regions of interest (morphology) are co-localized with Raman spectral data.

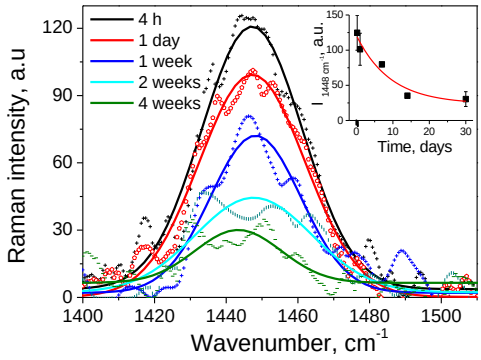

Figure 9. The differences in Raman band intensity at 1448 cm^{-1} of live dc3-f cells and dead cells stored at 4oC in 1x PBS for 1 day, 1 week, 2 weeks and 4 weeks.

Literature analysis revealed that following laser irradiation of biological sample, the signal to noise ratio of Raman spectra would increase thanks to decreased NIR autofluorescence intensity (photo-bleaching) [15]. The mechanism of cell and tissue autofluorescence photo-bleaching is still unclear. The main hypotheses considered in literature are: a) spontaneous fluorophore decomposition (after a number of absorption/emission cycles), b) destructive interactions with other dye-molecules and c) due to interaction with oxygen molecules and their derivatives. To check the hypothesis that intrinsic fluorophores of cells (NADH, flavines and lipopigments) play role as endogenous photosensitizers with subsequent production of singlet oxygen [16], in-vitro mouse melanoma cells b16f10 with attached singlet oxygen fluorescence sensor (SOSG) were irradiated by continuous laser irradiation (405 nm, power density 30 mW/cm^2) within 10 minutes. The obtained results (Fig.10.) demonstrate opposite trends of both fluorescence intensities over time. The decrease of cell's autofluorescence intensity can be well described by exponential decay with the rate constant τ_1 = 1.06 +/- 0.19 minutes while the SOSG fluorescence intensity increase was also exponential but slower, with the rate constant τ_2 = 2.6 +/- 1.15 minutes. One can assume that not only singlet oxygen is produced during the photo-bleaching but also radicals such as hydroxyl radicals, superoxide anion radicals, etc.

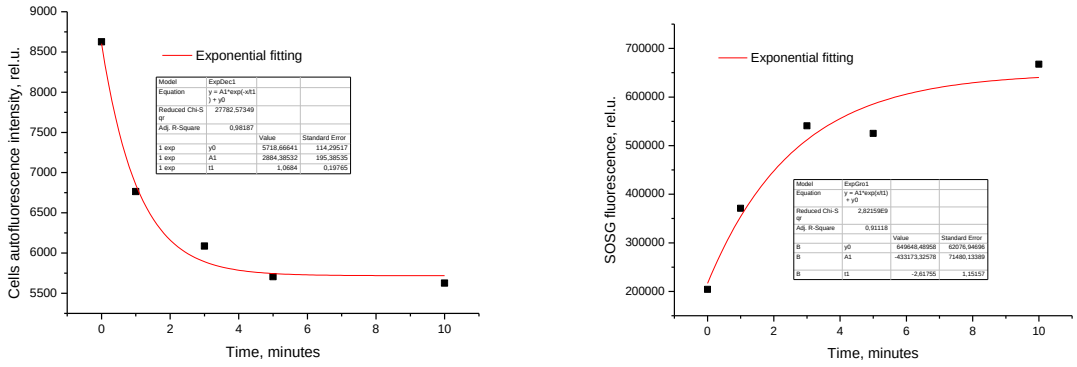

Figure 10. Left – melanoma cell autofluorescence intensity decrease during 10 minutes at 405nm continuous excitation measured at 480 nm band. Right – singlet oxygen fluorescence measured at 520nm band under 473nm excitation in the same experiment.

4. Summary

To summarize, the recent results of our lab on laser applications for skin assessment show a promising potential of the applied biophotonic methods. Results of the first systematic experimental study to determine spectral-spatial dependencies of skin-remitted photon path lengths by means of picosecond lasers have been reported [10]. Two design options for skin imaging with record high spectral selectivity using multi-laser illumination have been implemented in prototype devices [6,9]. A new research line – Raman skin spectroscopy and imaging – has been initiated. Raman macro-imaging can provide diagnostic criteria for the detection of skin malformations, attributed to changes in tissue structure and time course of lipid or protein degradation. However, more testing is necessary to demonstrate the reliability of this method. The strength of Raman macro imaging is ability to provide a wide field of view (~ cm^2), fast acquisition (10 seconds/image) and safe imaging conditions (< 300 mW/cm^2 power density). This method is still too complicated and expensive for immediate clinical applications but further research may explore ways for routine implementation in future. Finally, the obtained results on cell fluorescence photo-bleaching (Fig.10) will promote better understanding of the the mechanisms of skin autofluorescence photo-bleaching under laser excitation.

5. Acknowledgements

Authors would thank for the support provided by the European Regional Development Fund (projects No. 1.1.1.1/18/A/132, 1.1.1.2/VIAA/1/16/070 and 1.1.1.2/VIAA/1/16/014) and by the Latvian Council of Science (project No. lzp-2018/2-0006). The technical support of Dr. Ilona Kuzmina (preparation of the tissue phantoms) is highly appreciated.

References

[1] *Safety of Laser Products* - Part 1: Equipment Classification and Requirements IEC 60825-1, 2007.

[2] Ding H., Lu J. Q., Wooden W. A, Kragel P. J., Hu X.-H., "Refractive indices of human skin tissues at eight wavelengths and estimated dispersion relations between 300 and 1600 nm", *Phys.Med.Biol.* **51**(6), 1479-89 (2006).

[3] WO 2013135311 A1 (2012) "Method and device for imaging of spectral reflectance at several wavelength bands".

[4] Spigulis J., Elste L., "Single-snapshot RGB multispectral imaging at fixed wavelengths: proof of concept", Proc. SPIE **8937**, 89370L (2014).

[5] Spigulis J., "Multispectral, fluorescent and photoplethysmographic imaging for remote skin assessment", Sensors **17**, 1165 (2017).

[6] Spigulis J., Rupenheits Z., Matulenko M., Oshina I., Rubins U., "A snapshot multi-wavelengths imaging device for *in-vivo* skin diagnostics", *Proc.SPIE* **11232**, 112320I-1 (2020).

[7] Spigulis J., Oshina I., Berzina A., Bykov A., "Smartphone snapshot mapping of skin chromophores under triple-wavelength laser illumination", J.Biomed.Opt., **22**(9), 091508 (2017).

[8] Lihachev A., Lihacova I., Plorina E.V., Lange M., Derjabo A., Spigulis J., "Differentiation of seborrheic keratosis from basal cell carcinoma, nevi and melanoma by RGB autofluorescence imaging", Biomed.Opt.Expr., **9**(4), 1852-1858 (2018).

[9] Kviesis-Kipge E., "Development of skin chromophore mapping device using five spectral line illumination", *OSA Technical Digest* (Optical Society of America, 2019), ITh4B.3, https://doi.org/10.1364/ISA.2019.ITh4B.3.

[10] Lukinsone V., Maslobojeva A., Rubins U., Kuzminskis M., Osis M., Spigulis J., "Remitted photon path lengths in human skin: *in-vivo* measurement data", *Biomed.Opt.Expr.* **11**(5), 2866-2873 (2020). https://doi.org/10.1364/BOE.388349.

[11] Lukinsone V., Kuzmina I., Tamosiunas M., Maslobojeva A., Kuzminskis M., Rubins U., Spigulis J., "Remitted photon path length in human skin, skin phantoms and cell cultures", *Proc. SPIE* **11363**, 1136320 (2020). doi: 10.1117/12.2555822.
[12] Silveira, L., Pasqualucci, C.A., Bodanese, B. et al. Normal-subtracted preprocessing of Raman spectra aiming to discriminate skin actinic keratosis and neoplasias from benign lesions and normal skin tissues. Lasers Med Sci. **35**, 1141–1151 (2020); doi.org/10.1007/s10103-019-02935-w.
[13] Feng X, Moy AJ, Nguyen HTM, et al. Raman active components of skin cancer. Biomed Opt Express. **8**(6), 2835-2850 (2017); doi:10.1364/BOE.8.002835
[14] Kunapareddy N, Freyer JP, Mourant JR. Raman spectroscopic characterization of necrotic cell death. J Biomed Opt. **13**(5), 054002 (2008); doi:10.1117/1.2978061
[15] Bratchenko I.A., Artemyev D.N., Myakinin O.O., Khristoforova Y.A., Moryatov A.A., Kozlov S.V., Zakharov V.P.. "Combined Raman and autofluorescence ex vivo diagnostics of skin cancer in nearinfrared and visible regions". J Biomed Opt. **22**(2), 27005, 2017.
[16] Plavskii V.Yu et al., "Porphyrins and flavins as endogenous acceptors of optical radiation of blue spectral region determining photoinactivation of microbial cells", J.Photochem.Photobiol., **B183**,172-183 (2018).